EUROPEAN ORGANIZATION FOR NUCLEAR RESEARCH

CERN-EP-2000-90
July 7, 2000

Measurement of the $\mathrm{B^0}$ Lifetime and Oscillation Frequency using $\mathrm{\bar{B}^0 \to D^{*+}\ell^-\bar{\nu}}$ decays

The OPAL Collaboration

Abstract

The lifetime and oscillation frequency of the $\mathrm{B^0}$ meson has been measured using $\mathrm{\bar{B}^0 \to D^{*+}\ell^-\bar{\nu}}$ decays recorded on the $\mathrm{Z^0}$ peak with the OPAL detector at LEP. The $\mathrm{D^{*+} \to D^0\pi^+}$ decays were reconstructed using an inclusive technique and the production flavour of the $\mathrm{B^0}$ mesons was determined using a combination of tags from the rest of the event. The results

$$\begin{aligned} \tau_{\mathrm{B^0}} &= 1.541 \pm 0.028 \pm 0.023\,\mathrm{ps}\,, \\ \Delta m_{\mathrm{d}} &= 0.497 \pm 0.024 \pm 0.025\,\mathrm{ps}^{-1} \end{aligned}$$

were obtained, where in each case the first error is statistical and the second systematic.

Submitted to Physics Letters B.

The OPAL Collaboration

G. Abbiendi[2], K. Ackerstaff[8], C. Ainsley[5], P.F. Åkesson[3], G. Alexander[22], J. Allison[16], K.J. Anderson[9], S. Arcelli[17], S. Asai[23], S.F. Ashby[1], D. Axen[27], G. Azuelos[18,a], I. Bailey[26], A.H. Ball[8], E. Barberio[8], R.J. Barlow[16], S. Baumann[3], T. Behnke[25], K.W. Bell[20], G. Bella[22], A. Bellerive[9], G. Benelli[2], S. Bentvelsen[8], S. Bethke[32], O. Biebel[32], I.J. Bloodworth[1], O. Boeriu[10], P. Bock[11], J. Böhme[14,h], D. Bonacorsi[2], M. Boutemeur[31], S. Braibant[8], P. Bright-Thomas[1], L. Brigliadori[2], R.M. Brown[20], H.J. Burckhart[8], J. Cammin[3], P. Capiluppi[2], R.K. Carnegie[6], A.A. Carter[13], J.R. Carter[5], C.Y. Chang[17], D.G. Charlton[1,b], P.E.L. Clarke[15], E. Clay[15], I. Cohen[22], O.C. Cooke[8], J. Couchman[15], C. Couyoumtzelis[13], R.L. Coxe[9], A. Csilling[15,j], M. Cuffiani[2], S. Dado[21], G.M. Dallavalle[2], S. Dallison[16], A. de Roeck[8], E. de Wolf[8], P. Dervan[15], K. Desch[25], B. Dienes[30,h], M.S. Dixit[7], M. Donkers[6], J. Dubbert[31], E. Duchovni[24], G. Duckeck[31], I.P. Duerdoth[16], P.G. Estabrooks[6], E. Etzion[22], F. Fabbri[2], M. Fanti[2], L. Feld[10], P. Ferrari[12], F. Fiedler[8], I. Fleck[10], M. Ford[5], A. Frey[8], A. Fürtjes[8], D.I. Futyan[16], P. Gagnon[12], J.W. Gary[4], G. Gaycken[25], C. Geich-Gimbel[3], G. Giacomelli[2], P. Giacomelli[8], D. Glenzinski[9], J. Goldberg[21], C. Grandi[2], K. Graham[26], E. Gross[24], J. Grunhaus[22], M. Gruwé[25], P.O. Günther[3], C. Hajdu[29], G.G. Hanson[12], M. Hansroul[8], M. Hapke[13], K. Harder[25], A. Harel[21], M. Harin-Dirac[4], A. Hauke[3], M. Hauschild[8], C.M. Hawkes[1], R. Hawkings[8], R.J. Hemingway[6], C. Hensel[25], G. Herten[10], R.D. Heuer[25], J.C. Hill[5], A. Hocker[9], K. Hoffman[8], R.J. Homer[1], A.K. Honma[8], D. Horváth[29,c], K.R. Hossain[28], R. Howard[27], P. Hüntemeyer[25], P. Igo-Kemenes[11], K. Ishii[23], F.R. Jacob[20], A. Jawahery[17], H. Jeremie[18], C.R. Jones[5], P. Jovanovic[1], T.R. Junk[6], N. Kanaya[23], J. Kanzaki[23], G. Karapetian[18], D. Karlen[6], V. Kartvelishvili[16], K. Kawagoe[23], T. Kawamoto[23], R.K. Keeler[26], R.G. Kellogg[17], B.W. Kennedy[20], D.H. Kim[19], K. Klein[11], A. Klier[24], S. Kluth[32], T. Kobayashi[23], M. Kobel[3], T.P. Kokott[3], S. Komamiya[23], R.V. Kowalewski[26], T. Kress[4], P. Krieger[6], J. von Krogh[11], T. Kuhl[3], M. Kupper[24], P. Kyberd[13], G.D. Lafferty[16], H. Landsman[21], D. Lanske[14], I. Lawson[26], J.G. Layter[4], A. Leins[31], D. Lellouch[24], J. Letts[12], L. Levinson[24], R. Liebisch[11], J. Lillich[10], B. List[8], C. Littlewood[5], A.W. Lloyd[1], S.L. Lloyd[13], F.K. Loebinger[16], G.D. Long[26], M.J. Losty[7], J. Lu[27], J. Ludwig[10], A. Macchiolo[18], A. Macpherson[28,m], W. Mader[3], S. Marcellini[2], T.E. Marchant[16], A.J. Martin[13], J.P. Martin[18], G. Martinez[17], T. Mashimo[23], P. Mättig[24], W.J. McDonald[28], J. McKenna[27], T.J. McMahon[1], R.A. McPherson[26], F. Meijers[8], P. Mendez-Lorenzo[31], W. Menges[25], F.S. Merritt[9], H. Mes[7], A. Michelini[2], S. Mihara[23], G. Mikenberg[24], D.J. Miller[15], W. Mohr[10], A. Montanari[2], T. Mori[23], K. Nagai[8], I. Nakamura[23], H.A. Neal[12,f], R. Nisius[8], S.W. O'Neale[1], F.G. Oakham[7], F. Odorici[2], H.O. Ogren[12], A. Oh[8], A. Okpara[11], M.J. Oreglia[9], S. Orito[23], G. Pásztor[8,j], J.R. Pater[16], G.N. Patrick[20], J. Patt[10], P. Pfeifenschneider[14,i], J.E. Pilcher[9], J. Pinfold[28], D.E. Plane[8], B. Poli[2], J. Polok[8], O. Pooth[8], M. Przybycień[8,d], A. Quadt[8], C. Rembser[8], P. Renkel[24], H. Rick[4], N. Rodning[28], J.M. Roney[26], S. Rosati[3], K. Roscoe[16], A.M. Rossi[2], Y. Rozen[21], K. Runge[10], O. Runolfsson[8], D.R. Rust[12], K. Sachs[6], T. Saeki[23], O. Sahr[31], E.K.G. Sarkisyan[22], C. Sbarra[26], A.D. Schaile[31], O. Schaile[31], P. Scharff-Hansen[8], M. Schröder[8], M. Schumacher[25], C. Schwick[8], W.G. Scott[20], R. Seuster[14,h], T.G. Shears[8,k], B.C. Shen[4], C.H. Shepherd-Themistocleous[5], P. Sherwood[15], G.P. Siroli[2], A. Skuja[17], A.M. Smith[8], G.A. Snow[17], R. Sobie[26], S. Söldner-Rembold[10,e], S. Spagnolo[20], M. Sproston[20], A. Stahl[3], K. Stephens[16], K. Stoll[10], D. Strom[19], R. Ströhmer[31], L. Stumpf[26], B. Surrow[8], S.D. Talbot[1], S. Tarem[21], R.J. Taylor[15], R. Teuscher[9], M. Thiergen[10], J. Thomas[15], M.A. Thomson[8], E. Torrence[9], S. Towers[6], D. Toya[23], T. Trefzger[31], I. Trigger[8], Z. Trócsányi[30,g], E. Tsur[22], M.F. Turner-Watson[1], I. Ueda[23], B. Vachon26, P. Vannerem[10], M. Verzocchi[8], H. Voss[8], J. Vossebeld[8], D. Waller[6], C.P. Ward[5], D.R. Ward[5], P.M. Watkins[1], A.T. Watson[1], N.K. Watson[1], P.S. Wells[8], T. Wengler[8], N. Wermes[3], D. Wetterling[11] J.S. White[6], G.W. Wilson[16], J.A. Wilson[1], T.R. Wyatt[16], S. Yamashita[23], V. Zacek[18], D. Zer-Zion[8,l]

[1]School of Physics and Astronomy, University of Birmingham, Birmingham B15 2TT, UK
[2]Dipartimento di Fisica dell' Università di Bologna and INFN, I-40126 Bologna, Italy
[3]Physikalisches Institut, Universität Bonn, D-53115 Bonn, Germany
[4]Department of Physics, University of California, Riverside CA 92521, USA
[5]Cavendish Laboratory, Cambridge CB3 0HE, UK
[6]Ottawa-Carleton Institute for Physics, Department of Physics, Carleton University, Ottawa, Ontario K1S 5B6, Canada
[7]Centre for Research in Particle Physics, Carleton University, Ottawa, Ontario K1S 5B6, Canada
[8]CERN, European Organisation for Nuclear Research, CH-1211 Geneva 23, Switzerland
[9]Enrico Fermi Institute and Department of Physics, University of Chicago, Chicago IL 60637, USA
[10]Fakultät für Physik, Albert Ludwigs Universität, D-79104 Freiburg, Germany
[11]Physikalisches Institut, Universität Heidelberg, D-69120 Heidelberg, Germany
[12]Indiana University, Department of Physics, Swain Hall West 117, Bloomington IN 47405, USA
[13]Queen Mary and Westfield College, University of London, London E1 4NS, UK
[14]Technische Hochschule Aachen, III Physikalisches Institut, Sommerfeldstrasse 26-28, D-52056 Aachen, Germany
[15]University College London, London WC1E 6BT, UK
[16]Department of Physics, Schuster Laboratory, The University, Manchester M13 9PL, UK
[17]Department of Physics, University of Maryland, College Park, MD 20742, USA
[18]Laboratoire de Physique Nucléaire, Université de Montréal, Montréal, Quebec H3C 3J7, Canada
[19]University of Oregon, Department of Physics, Eugene OR 97403, USA
[20]CLRC Rutherford Appleton Laboratory, Chilton, Didcot, Oxfordshire OX11 0QX, UK
[21]Department of Physics, Technion-Israel Institute of Technology, Haifa 32000, Israel
[22]Department of Physics and Astronomy, Tel Aviv University, Tel Aviv 69978, Israel
[23]International Centre for Elementary Particle Physics and Department of Physics, University of Tokyo, Tokyo 113-0033, and Kobe University, Kobe 657-8501, Japan
[24]Particle Physics Department, Weizmann Institute of Science, Rehovot 76100, Israel
[25]Universität Hamburg/DESY, II Institut für Experimental Physik, Notkestrasse 85, D-22607 Hamburg, Germany
[26]University of Victoria, Department of Physics, P O Box 3055, Victoria BC V8W 3P6, Canada
[27]University of British Columbia, Department of Physics, Vancouver BC V6T 1Z1, Canada
[28]University of Alberta, Department of Physics, Edmonton AB T6G 2J1, Canada
[29]Research Institute for Particle and Nuclear Physics, H-1525 Budapest, P O Box 49, Hungary
[30]Institute of Nuclear Research, H-4001 Debrecen, P O Box 51, Hungary
[31]Ludwigs-Maximilians-Universität München, Sektion Physik, Am Coulombwall 1, D-85748 Garching, Germany
[32]Max-Planck-Institute für Physik, Föhring Ring 6, 80805 München, Germany

[a] and at TRIUMF, Vancouver, Canada V6T 2A3
[b] and Royal Society University Research Fellow
[c] and Institute of Nuclear Research, Debrecen, Hungary
[d] and University of Mining and Metallurgy, Cracow
[e] and Heisenberg Fellow
[f] now at Yale University, Dept of Physics, New Haven, USA
[g] and Department of Experimental Physics, Lajos Kossuth University, Debrecen, Hungary
[h] and MPI München
[i] now at MPI für Physik, 80805 München
[j] and Research Institute for Particle and Nuclear Physics, Budapest, Hungary
[k] now at University of Liverpool, Dept of Physics, Liverpool L69 3BX, UK
[l] and University of California, Riverside, High Energy Physics Group, CA 92521, USA
[m] and CERN, EP Div, 1211 Geneva 23.

1 Introduction

The lifetimes of b hadrons depend both on the strength of the b quark coupling to the lighter c and u quarks, and on the dynamics of b hadron decay. The spectator model prediction that the lifetimes of all heavy hadrons containing the same heavy quark are equal is modified by non-spectator effects dependent on the flavour of the light quark(s) in the hadron. In contrast to the charm hadrons, where $\tau_{D^+} \approx 2.5\tau_{D^0}$ [1], non-spectator processes are expected to lead to lifetime differences between the B^+ and B^0 mesons of at most 10 % [2]. Measurements of b hadron lifetimes at the level of a few percent or better are therefore needed to test these predictions, and probe the non-spectator processes contributing to the decays. In addition, precise measurements of the B^0 lifetime are also needed for the determination of the magnitude of the CKM matrix element V_{cb} [3].

The most precise measurements of the B^+ lifetime come from topological vertex reconstruction techniques, where the selection of charged secondary vertices allows a clean sample of B^+ decays to be isolated [4,5]. This method is however limited for B^0 lifetime measurements, due to contamination from other neutral b hadrons (B_s mesons and b baryons). An alternative technique is to use $\bar{B}^0 \to D^{*+}\ell^-\bar{\nu}$ decays[1], which can be efficiently partially reconstructed by exploiting the low energy release in the decay $D^{*+} \to D^0\pi^+$. In this case, only the π^+ from the D^{*+} decay is identified, and no attempt is made to fully reconstruct the D^0 meson decay. This method has previously been used by DELPHI [6] to measure the B^0 lifetime, and by DELPHI [7] and OPAL [8] to measure $|V_{cb}|$.

The same sample of $\bar{B}^0 \to D^{*+}\ell^-\bar{\nu}$ decays can also be used to measure the B^0-$\bar{B}^0$ oscillation frequency[2] Δm_d [9]. In the neutral b meson system, the weak eigenstates B^0 and $\bar{B}^0$ differ from the mass eigenstates, and transitions between them are possible, arising dominantly in the Standard Model from second order weak transition box diagrams involving virtual top quarks. Therefore an initial B^0 meson can oscillate into a $\bar{B}^0$ at time t with a probability given by

$$P(B^0 \to \bar{B}^0) = \frac{1}{2}(1 - \cos \Delta m_d t) \, .$$

Measurements of Δm_d allow the extraction of the magnitude of the CKM matrix element V_{td}, though the precision is currently severely limited by theoretical uncertainties [10].

In this paper, measurements of both τ_{B^0} and Δm_d based on this technique are presented. The reconstruction of $\bar{B}^0 \to D^{*+}\ell^-\bar{\nu}$ decays is described in Section 2, followed by the determination of the proper decay time for each event in Section 3, and the production flavour tagging needed for the oscillation measurement in Section 4. The fit to determine τ_{B^0} and Δm_d is described in Section 5, followed by a discussion of systematic uncertainties in Section 6. The results are summarised and combined with previous OPAL measurements in Section 7.

2 Inclusive reconstruction of $\bar{B}^0 \to D^{*+}\ell^-\bar{\nu}$ events

The OPAL detector is well described elsewhere [11]. The data sample used in this analysis consists of about 4 million hadronic Z^0 decays collected during the period 1991–1995, together with an additional 400 000 events recorded primarily for detector calibration purposes in 1996–2000. Corresponding simulated event samples were generated using JETSET 7.4 [12] as described in [13].

Hadronic Z^0 decays were selected using standard criteria [13]. To ensure the event was well contained within the acceptance of the detector, the thrust axis direction[3] was required to satisfy $|\cos\theta_T| < 0.9$. Tracks and electromagnetic calorimeter clusters with no associated tracks were then combined into jets using a cone algorithm [14], with a cone half-angle of 0.65 rad and a minimum jet

[1] Charge conjugate reactions are implied, and the symbol ℓ refers to either an electron or muon.

[2] The conventions $c = 1$ and $\hbar = 1$ are employed throughout.

[3] A right handed coordinate system is used, with positive z along the electron beam direction and x pointing to the centre of the LEP ring. The polar and azimuthal angles are denoted by θ and ϕ.

energy of 5 GeV. The transverse momentum p_t of each track was defined relative to the axis of the jet containing it, where the jet axis was calculated including the momentum of the track.

The reconstruction of $\bar{\mathrm{B}}^0 \to \mathrm{D}^{*+}\ell^-\bar{\nu}$ events was performed by combining high p and p_t lepton (electron or muon) candidates with oppositely charged pions from the $\mathrm{D}^{*+} \to \mathrm{D}^0\pi^+$ decay. The selection is similar to that used in [8], but with some changes to produce an unbiased B^0 decay proper time measurement and to increase the efficiency at the expense of higher combinatorial background. Electrons were identified and photon conversions rejected using neural network algorithms [13], and muons were identified as in [15]. Both electrons and muons were required to have momenta $p > 2\,\mathrm{GeV}$, transverse momenta with respect to the jet axis $p_t > 0.7\,\mathrm{GeV}$, and to lie in the polar angle region $|\cos\theta| < 0.9$.

The selection of pions from D^{*+} decays relies on the small mass difference of only 145 MeV [1] between the D^{*+} and D^0, which means the pions have very little transverse momentum with respect to the D^0 direction. In each jet containing a lepton candidate, the D^0 momentum vector $\mathbf{p}_{\mathrm{D}^0}$ and energy E_{D^0} were reconstructed using an inclusive technique, selecting a group of tracks and calorimeter clusters compatible with a D^0 decay using kinematic, impact parameter and invariant mass information. This procedure is described fully in [8] and gives angular resolutions on the D^0 direction of about 45 mrad in both θ and ϕ.

Each track in the jet (other than the lepton) was then considered in turn as a slow pion candidate, provided it satisfied $0.5\,\mathrm{GeV} < p < 2.5\,\mathrm{GeV}$ and had a transverse momentum with respect to the D^0 direction of less than 0.3 GeV. If the pion under consideration had been included in the reconstructed D^0, it was removed and the D^0 momentum and energy recalculated. The final selection was made using the reconstructed mass difference[4] ΔM between the D^{*+} and D^0 mesons, calculated as

$$\Delta M = \sqrt{E^2_{\mathrm{D}^*} - |\mathbf{p}_{\mathrm{D}^*}|^2} - m_{\mathrm{D}^0}\,,$$

where the D^{*+} energy is given by $E_{\mathrm{D}^*} = E_{\mathrm{D}^0} + E_\pi$ and momentum by $\mathbf{p}_{\mathrm{D}^*} = \mathbf{p}_{\mathrm{D}^0} + \mathbf{p}_\pi$.

The position of the B^0 candidate decay vertex was reconstructed from the intersection point of the lepton and slow pion tracks in the x-y plane. The two-dimensional flight distance of the B^0 was then calculated as the length of the vector between the $\mathrm{e}^+\mathrm{e}^-$ interaction point ('beamspot') and the B^0 decay vertex, constrained to lie along the x-y projection of the jet direction. This was converted to a three dimensional decay distance L using the jet polar angle. Using just the lepton and pion tracks, together with the interaction point position and uncertainty determined with a fit to many consecutive events [16], results in a decay length estimate which is bias free and whose resolution does not depend strongly on the decay length itself. Although the decay length resolution could be improved by adding more tracks to the B^0 decay vertex, this would introduce significant bias at small decay lengths, and is not necessary as the resolution is already adequate for the measurement of τ_{B^0} and Δm_{d}.

The reconstructed decay length L was signed positive if the B^0 decay vertex was displaced from the beamspot in the direction of the jet momentum, and negative otherwise. The decay length error σ_L was calculated from the track parameter and beamspot position error matrices. The decay length and error were required to satisfy $-0.5\,\mathrm{cm} < L < 2\,\mathrm{cm}$, $L/\sigma_L > -3$ and $\sigma_L < 0.2\,\mathrm{cm}$.

The resulting distributions of ΔM for opposite and same sign lepton-pion combinations are shown in Figure 1(a) and (b). The predictions of the Monte Carlo simulation are also shown, broken down into contributions from signal $\bar{\mathrm{B}}^0 \to \mathrm{D}^{*+}\ell^-\bar{\nu}$ events, 'resonant' background containing real leptons combined with slow pions from D^{*+} decays, and combinatorial background, made up of events with fake slow pions, fake leptons or both.

In Monte Carlo simulation, about 36 % of opposite sign events with $\Delta M < 0.17\,\mathrm{GeV}$ are signal $\bar{\mathrm{B}}^0 \to \mathrm{D}^{*+}\ell^-\bar{\nu}$ events, 15 % are resonant background and 49 % are combinatorial background. The resonant background is made up mainly of $\mathrm{B}^- \to \mathrm{D}^{*+}\pi^-\ell^-\bar{\nu}$, $\bar{\mathrm{B}}^0 \to \mathrm{D}^{*+}\pi^0\ell^-\bar{\nu}$ and $\bar{\mathrm{B}}_{\mathrm{s}} \to \mathrm{D}^{*+}\mathrm{K}^0\ell^-\bar{\nu}$ decays. These are expected to be dominated by b semileptonic decays involving orbitally excited

[4] The D^{*+}–D^0 mass difference ΔM was denoted by Δm in [8].

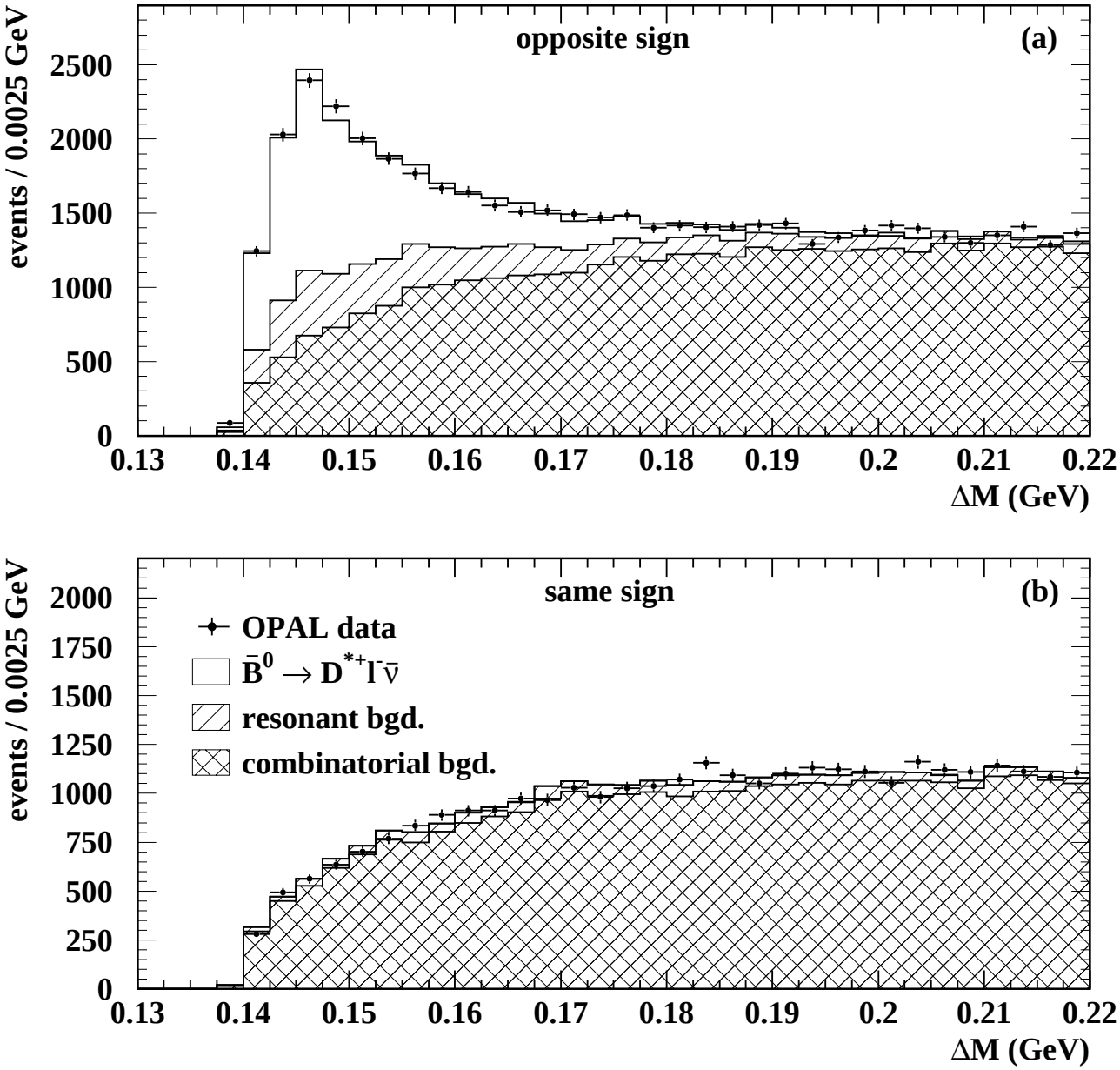

Figure 1: Reconstructed ΔM distributions for selected (a) opposite sign and (b) same sign lepton-pion combinations. The data are shown by the points with error bars, and the Monte Carlo simulation contributions from signal $\bar{\mathrm{B}}^0 \to \mathrm{D}^{*+}\ell^-\bar{\nu}$ decays, other resonant D^{*+} decays and combinatorial background are shown by the open, single and cross hatched histograms respectively.

charm mesons (generically referred to as D^{**}), *e.g.* $B^- \to D^{**0}\ell^-\bar{\nu}$ followed by $D^{**0} \to D^{*+}\pi^-$. These decays will be denoted collectively by $\bar{B} \to D^{*+}h\,\ell^-\bar{\nu}$. Small contributions are also expected from $b \to D^{*+}\tau\bar{\nu}X$ decays (via any b hadron) with the τ decaying leptonically, and $b \to D^{*+}D_s^-X$ with the D_s^- decaying semileptonically (each about 1 % of opposite sign events). For same sign events with $\Delta M < 0.17\,\mathrm{GeV}$, there is a small resonant contribution of about 6 % from events with a real $D^{*+} \to D^0\pi^+$ where the D^0 decays semileptonically, and the rest is combinatorial background.

3 Proper time reconstruction

The proper decay time t of each B^0 candidate was calculated from its reconstructed decay length L and energy E_{B^0}. The energy was calculated using a technique similar to that described in [17], exploiting overall energy and momentum conservation in the event to account for the missing energy of the unreconstructed neutrino. The event was treated as a two-body decay of a Z^0 into a B^0 of mass 5.279 GeV [1] and another object making up the rest of the event. The B^0 energy was calculated as

$$E_{B^0} = \frac{E_{\mathrm{cm}}^2 + m_{B^0}^2 - M_{\mathrm{rec}}^2}{2E_{\mathrm{cm}}}$$

where E_{cm} is the centre-of-mass energy of the event and M_{rec} the invariant mass of the object recoiling against the B^0. The latter was calculated from all tracks and calorimeter clusters in the event, excluding the lepton and those associated to the reconstructed D^{*+}. A correction for double counting of charged particles in the tracking detectors and calorimeters was applied [18], and the recoil mass was first scaled by $(\bar{E}/E_{\mathrm{vis}})$ where E_{vis} is the total event visible energy and $\bar{E} = 87\,\mathrm{GeV}$ is the typical visible energy in events with only one neutrino. This procedure improves the resolution in events where a second neutrino is present [19]. The resulting energy estimate is unbiased and has an RMS resolution of 3.8 GeV in Monte Carlo $\bar{B}^0 \to D^{*+}\ell^-\bar{\nu}$ events, as shown in Figure 2(a).

The proper decay time t was then calculated from the candidate decay length and energy as

$$t = \frac{m_{B^0} L}{\sqrt{E_{B^0}^2 - m_{B^0}^2}}\,.$$

The resulting proper time resolution depends on the true proper time t', but has no significant bias, as shown in Figure 2(b–f). The resolution degrades with increasing proper time due to the larger influence of the energy resolution at large decay lengths. The resolution was parameterised as a function $R_{D^{*+}}(t,t')$ giving the expected distribution of reconstructed t for each true value t'. The resolution function was implemented as the sum of three Gaussian distributions, whose widths vary linearly with t'. The resolution function is also shown as the solid line in Figure 2(b–f), and gives a reasonable description of the Monte Carlo resolution, adequate for measuring the lifetime and relatively slow B^0 meson oscillations.

Similar resolution functions $R_{D^{*+}\pi^-}(t,t')$, $R_{D^{*+}\pi^0}(t,t')$ and $R_{D^{*+}K^0}(t,t')$ were generated for the three main D^{**} background contributions $B^- \to D^{*+}\pi^-\ell^-\bar{\nu}$, $\bar{B}^0 \to D^{*+}\pi^0\ell^-\bar{\nu}$ and $\bar{B}_s \to D^{*+}K^0\ell^-\bar{\nu}$. In these events, the b hadron energy reconstruction has a bias of about $-1.5\,\mathrm{GeV}$ as some of the b hadron decay products are incorrectly included in the recoil mass. This bias was corrected in the corresponding resolution functions.

4 Production flavour tagging

The B^0 oscillation frequency measurement requires that the production and decay flavour (B^0 or $\bar{B}^0$) of each meson be determined, in addition to the decay proper time t. The decay flavour can be determined from the sign of the lepton in the $\bar{B}^0 \to D^{*+}\ell^-\bar{\nu}$ decay, but the production flavour must be determined from other information in the event. The production of quark anti-quark pairs in

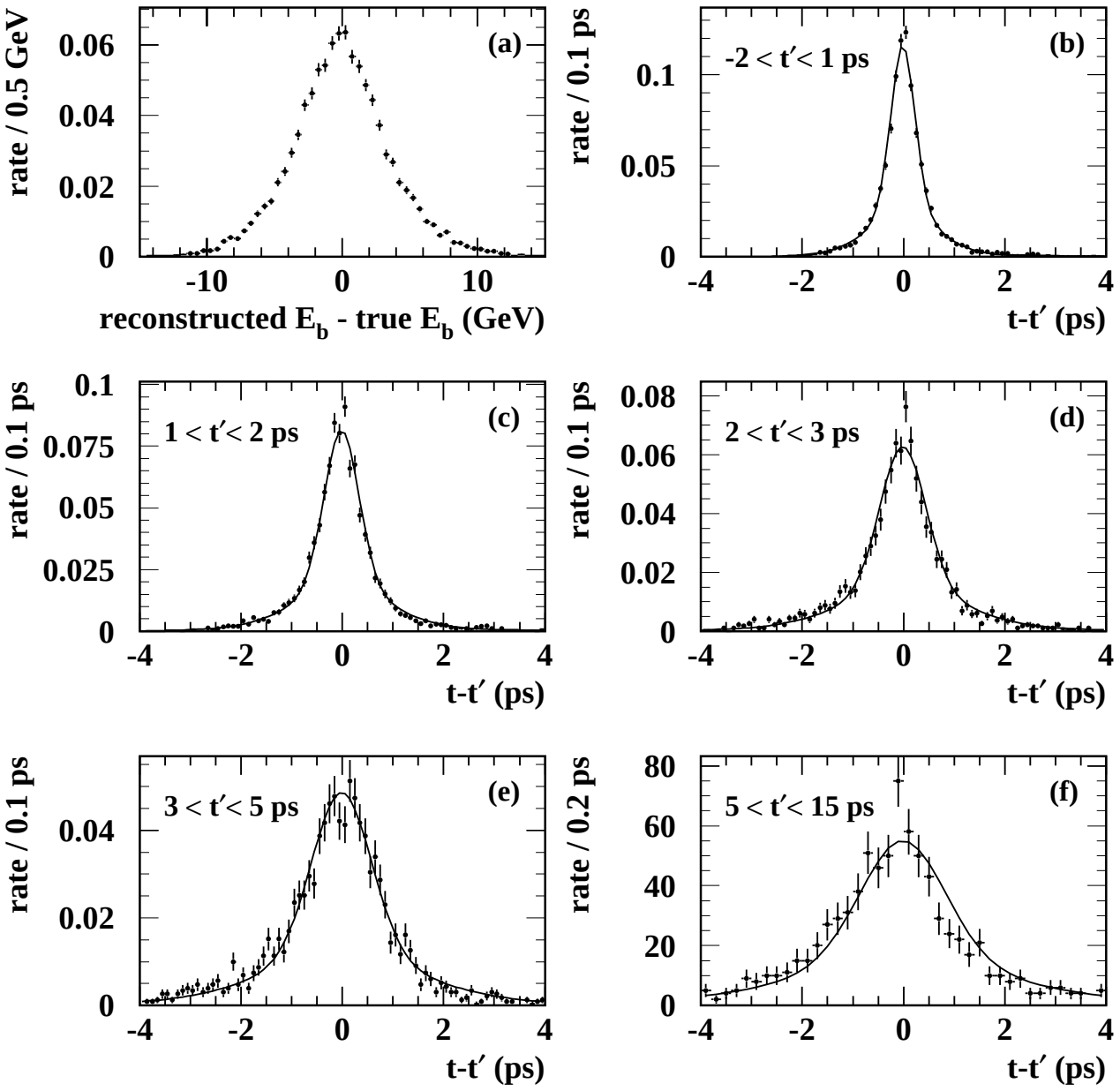

Figure 2: (a) Reconstructed b hadron energy resolution and (b–f) reconstructed proper time resolution in various ranges of true proper time t', for Monte Carlo $\bar{B}^0 \to D^{*+}\ell^-\bar{\nu}$ events. The Monte Carlo is shown by the points with error bars, and the resolution function is shown by the solid line in (b–f).

$Z^0 \to b\overline{b}$ decays allows the production flavour of the B^0 to be inferred from that of the other b hadron in the event. This information is diluted due to the possible mixing of the second b hadron. The other particles in the B^0 jet (produced in the fragmentation of the b quark) also carry some useful information.

The tagging information was extracted using the methods described in [4, 20]. The event was divided into two hemispheres by the plane perpendicular to the thrust axis and containing the e^+e^- interaction point. In the hemisphere opposite to that containing the B^0 jet, up to three pieces of information were used to tag the b hadron flavour:

- The jet charge $Q_{\rm opp}$ of the highest energy jet in the opposite hemisphere, defined as

$$Q_{\rm opp} = \frac{\sum_i (p_i^l)^\kappa q_i}{\sum_i (p_i^l)^\kappa} \tag{1}$$

  where p_i^l is the longitudinal momentum component with respect to the jet axis and q_i the charge of track i, and the sum is taken over all tracks in the jet. The parameter κ was set to 0.5, as in [20].

- The charge $Q_{\rm vtx}$ of a secondary vertex (if existing), reconstructed in any jet in the opposite hemisphere, as in [4]. A well reconstructed charged vertex indicates a B^+ or B^- hadron, tagging the parent quark as a $\overline{\rm b}$ or b respectively, whilst a neutral or badly reconstructed vertex gives no information on the b quark flavour.

- The charge of a high momentum lepton found in any jet in the opposite hemisphere, selected as in [4]. A high momentum lepton is most likely to come from a b hadron decay, again tagging the parent b or $\overline{\rm b}$ quark according to its charge. A neural network algorithm was used to suppress fake leptons and those coming from cascade charm decays ($b \to c \to \ell$) which have the wrong charge correlation.

These variables were combined using a neural network algorithm into a single tagging variable $Q_{\rm T}$ for the opposite hemisphere [4, 20], quantifying the confidence with which the hemisphere was tagged as containing a b or $\overline{\rm b}$ hadron. Different neural networks were used depending on what combination of vertex and/or lepton variables were available to combine with the jet charge $Q_{\rm opp}$.

In the hemisphere containing the B^0 jet, only the jet charge $Q_{\rm same}$ can be used to infer the B^0 production flavour. $Q_{\rm same}$ was calculated using equation 1, but with the parameter κ set to zero, so it becomes simply the average of the charges of the tracks in the jet. This avoids being sensitive to the decay flavour of the B^0 (and hence whether it has mixed or not), but is still sensitive to the production flavour via the information carried by the fragmentation tracks in the jet [21]. The jet charge $Q_{\rm same}$ was used to generate a second hemisphere tagging variable $Q_{\rm M}$ independent of the opposite hemisphere variable $Q_{\rm T}$.

The two tagging variables were combined to produce a single tag Q_2 for the B^0 production flavour, as in [4]. The continuous variable Q_2 ranges from -1 to $+1$, and is defined such that events with $Q_2 = +1$ are tagged with complete confidence as containing a produced B^0, events with $Q_2 = -1$ are tagged with complete confidence as containing a produced $\bar{B}^0$, and events with $Q_2 = 0$ are equally likely to be B^0 or $\bar{B}^0$. The modulus $|Q_2|$ satisfies $|Q_2| = 1 - 2\eta$, where η is the 'mis-tag' probability, *i.e.* the probability to tag the production flavour incorrectly. Finally, the production flavour tag Q_2 and B^0 decay lepton sign l were combined to produce the mixing tag $Q = Q_2 \cdot l$, such that events with $Q > 0$ ($Q < 0$) are tagged as unmixed (mixed).

Both the sign and magnitude of Q are used in the fit to determine $\Delta m_{\rm d}$, giving the events with high probability to be correctly tagged more weight. Considering only the sign of Q, 31 % of signal events are tagged incorrectly. The event-by-event weighting reduces this to an effective mis-tag of 28 %, equivalent to a 33 % increase in statistical sensitivity.

5 Fit and results

The values of τ_{B^0} and Δm_{d} were extracted using an unbinned extended maximum likelihood fit to the reconstructed mass difference ΔM, proper time t and mixing tag Q of each event. Both opposite and same sign events with $\Delta M < 0.22\,\mathrm{GeV}$ and $-2 < t < 15\,\mathrm{ps}$ were used in the fit, the high ΔM and same sign events serving to constrain the combinatorial background normalisation and shapes in the opposite sign low ΔM region populated by the $\bar{\mathrm{B}}^0 \to \mathrm{D}^{*+}\ell^-\bar{\nu}$ decays. Using the ΔM value from each event in the fit, rather than just dividing the data into low ΔM 'signal' and high ΔM 'sideband' mass regions, increases the statistical sensitivity as the signal purity varies considerably within the low ΔM region.

The likelihood is similar to that used in [8] for the measurement of $|V_{\mathrm{cb}}|$. The logarithm of the overall likelihood was given by

$$\ln \mathcal{L} = \sum_{i=1}^{M^a} \ln \mathcal{L}_i^a + \sum_{j=1}^{M^b} \ln \mathcal{L}_j^b - N^a - N^b \tag{2}$$

where the sums of individual event log-likelihoods $\ln \mathcal{L}_i^a$ and $\ln \mathcal{L}_j^b$ are taken over all the observed M^a opposite sign and M^b same sign events in the data sample, and N^a and N^b are the corresponding expected numbers of events.

The likelihood for each opposite sign event was given in terms of different types or sources of event by

$$\mathcal{L}_i^a(\Delta M_i, t_i, Q_i) = \sum_{s=1}^{4} N_s^a M_s(\Delta M_i)\, T_s(t_i, Q_i) \tag{3}$$

where N_s^a is the number of expected events, $M_s(\Delta M)$ the mass difference distribution and $T_s(t, Q)$ the proper time distribution for source s. For each source, the mass difference distribution $M_s(\Delta M)$ is normalised to one. The total number of expected events is given by the sum of the individual contributions: $N^a = \sum_{s=1}^{4} N_s^a$.

There are four opposite sign sources: (1) signal $\bar{\mathrm{B}}^0 \to \mathrm{D}^{*+}\ell^-\bar{\nu}$ events, (2) $\bar{\mathrm{B}} \to \mathrm{D}^{*+}\mathrm{h}\,\ell^-\bar{\nu}$ events where the D^{*+} is produced via an intermediate D^{**}, (3) other opposite sign background involving a genuine lepton and a slow pion from D^{*+} decay and (4) combinatorial background. The sum of sources 2 and 3 are shown as 'resonant background' in Figure 1. A similar expression to equation 3 was used for $\mathcal{L}_j^b$, the event likelihood for same sign events. In this case, only sources 3 and 4 contribute.

The mass difference distributions $M_s(\Delta M)$ for sources 1–3 were represented by analytic functions, whose parameters were determined using large numbers of simulated events. For the signal (source 1), both unmixed and mixed events must be considered to determine the proper time distribution $T_1(t, Q)$. The probability to find a signal decay with true proper time t' is given by:

$$P_1(t', Q) = \frac{1}{\tau_{\mathrm{B}^0}}\, e^{-t'/\tau_{\mathrm{B}^0}} \left(P_{\mathrm{u}}(Q) \frac{(1 + \cos \Delta m_{\mathrm{d}} t')}{2} + P_{\mathrm{m}}(Q) \frac{(1 - \cos \Delta m_{\mathrm{d}} t')}{2} \right)$$

where P_{u} (P_{m}) is the probability that the event is unmixed (mixed) given the observed mixing tag Q. These probabilities are given by $P_{\mathrm{u}}(Q) = (1 + Q)/2$ and $P_{\mathrm{m}}(Q) = (1 - Q)/2$. The signal probability is then convolved with the time resolution function $R_{\mathrm{D}^{*+}}(t, t')$ described in Section 3 to give the expected reconstructed proper time distribution $T_1(t, Q)$ as a function of the assumed B^0 lifetime τ_{B^0} and oscillation frequency Δm_{d}:

$$T_1(t, Q) = \int_0^\infty dt' \frac{1}{2\tau_{\mathrm{B}^0}}\, e^{-t'/\tau_{\mathrm{B}^0}} (1 + Q \cos \Delta m_{\mathrm{d}} t') R_{\mathrm{D}^{*+}}(t, t')\,. \tag{4}$$

The corresponding proper time distribution $T_2(t, Q)$ for source 2 (D^{**}) was calculated from the sum of the individual contributions from B^+, B^0 and $\mathrm{B_s}$ decays via D^{**}. For B^0 and $\mathrm{B_s}$ decays, equation 4 was

Quantity	Assumed value	Reference
τ_{B^+}	$1.65 \pm 0.03\,\mathrm{ps}$	[22]
$\tau_{\mathrm{B_s}}$	$1.54 \pm 0.07\,\mathrm{ps}$	[1]
Δm_{s}	9.1–$50\,\mathrm{ps}^{-1}$	[22], see text
R_{b}	$(21.70 \pm 0.09)\,\%$	[1]
$\mathrm{Br}(\mathrm{D}^{*+} \to \mathrm{D}^0\pi^+)$	$(68.3 \pm 1.4)\,\%$	[1]
$\mathrm{Br}(\mathrm{b} \to \mathrm{D}^{*+}\mathrm{h}\,\ell\bar{\nu})$	$(0.76 \pm 0.16)\,\%$	[23, 8]
$\mathrm{Br}(\mathrm{b} \to \mathrm{D}^{*+}\tau^-\bar{\nu}\mathrm{X})$	$(0.65 \pm 0.13)\,\%$	[1, 8]
$\mathrm{Br}(\bar{\mathrm{B}}^0 \to \mathrm{D}^{*+}\mathrm{D}_{\mathrm{s}}^{(*)-})$	$(4.2 \pm 1.5)\,\%$	[1]
$\mathrm{Br}(\mathrm{b} \to \mathrm{D}^{*+}\mathrm{X})$	$(17.3 \pm 2.0)\,\%$	[24]
$\mathrm{Br}(\mathrm{c} \to \mathrm{D}^{*+}\mathrm{X})$	$(22.2 \pm 2.0)\,\%$	[24]

Table 1: Input quantities used in the fit for τ_{B^0} and Δm_{d}.

modified, with the resolution function $R_{\mathrm{D}^{*+}}(t,t')$ replaced by $R_{\mathrm{D}^{*+}\pi^0}(t,t')$ (B^0 decays) or $R_{\mathrm{D}^{*+}\mathrm{K}^0}(t,t')$ ($\mathrm{B_s}$ decays), and τ_{B^0} and Δm_{d} replaced by $\tau_{\mathrm{B_s}}$ and Δm_{s}, the $\mathrm{B_s}$ lifetime and oscillation frequency, for $\mathrm{B_s}$ decays. For B^+ decays, which are always unmixed, the proper time distribution takes the form

$$T_{2,\mathrm{B}^+}(t,Q) = \int_0^\infty dt' \frac{1}{2\tau_{\mathrm{B}^+}}\, e^{-t'/\tau_{\mathrm{B}^+}} (1+Q) R_{\mathrm{D}^{*+}\pi^-}(t,t')\,.$$

The values of τ_{B^+}, $\tau_{\mathrm{B_s}}$ and Δm_{s} and their corresponding uncertainties were taken from [1, 22] and are given in Table 1; Δm_{s} was varied between the experimental lower limit and $50\,\mathrm{ps}^{-1}$, well above the experimental sensitivity and theoretically favoured region.

The number of signal events N_1^a was left as a free parameter in the fit. The number of events in source 2, and the relative contributions of B^+, B^0 and $\mathrm{B_s}$ decays within this source, were calculated as described in [8], from the measured branching ratio $\mathrm{Br}(\mathrm{b} \to \mathrm{D}^{*+}\pi^-\ell\bar{\nu}\mathrm{X}) = (0.473 \pm 0.095)\,\%$ [23] and the assumption of isospin and SU(3) symmetry. This was combined with the selection efficiency estimated from Monte Carlo and the values of R_{b} and $\mathrm{Br}(\mathrm{D}^{*+} \to \mathrm{D}^0\pi^+)$ listed in Table 1 to determine the expected number of these events in the data sample.

The numbers $N_3^{a,b}$ of events in the small background contributions covered by source 3 (both opposite and same sign) were taken from Monte Carlo simulation, with branching ratios adjusted to the values given in Table 1, as described in more detail in [8]. The proper time distributions $T_3(t,Q)$ were described by negative exponentials convolved with Gaussian resolution functions, with parameters again determined from Monte Carlo, as were the fractions of mixed events in each contribution.

The parameters of the analytic functions describing the combinatorial background (N_4^a, N_4^b, $M_4(\Delta M)$ and $T_4(t,Q)$ were fitted entirely from the data, with only the choice of functional forms motivated by simulation. The shapes of the mass and proper time functions (including a small correlation between ΔM and t) are constrained by the same sign sample (which is almost entirely combinatorial background), and the opposite sign high ΔM region serves to normalise the number of combinatorial background events in the low ΔM region. Since the combinatorial background is dominated by semileptonic b decays, it contains oscillating components in both opposite and same sign samples. The amplitude and frequency of this oscillation were constrained to be the same in both samples, but the fraction of unmixed events was allowed to be different, as supported by Monte Carlo simulation studies.

The values of τ_{B^0} and Δm_{d} were extracted by maximising the total likelihood given by equation 2. The values of τ_{B^0} and Δm_{d} were allowed to vary, together with the number of signal events and 18 auxiliary parameters describing the combinatorial background level, mass difference, time and mixing distributions. A result of

$$\begin{aligned} \tau_{\mathrm{B}^0} &= 1.541 \pm 0.028\,\mathrm{ps}\,, \\ \Delta m_{\mathrm{d}} &= 0.497 \pm 0.024\,\mathrm{ps}^{-1} \end{aligned}$$

Error Source	$\Delta(\tau_{B^0})$ (ps)	$\Delta(\Delta m_d)$ (ps^{-1})
B^+ lifetime	0.004	0.001
B_s lifetime	0.002	0.001
$Br(b \to D^{*+}\tau^-\bar{\nu})$	0.001	0.001
$Br(b \to D^{*+}D_s^{(*)-})$	0.005	0.002
$Br(b \to D^{*+}X)$	0.001	0.001
$b \to D^{**}\ell\bar{\nu}X$ decays	0.004	0.009
Other backgrounds	0.006	0.005
b fragmentation	0.005	0.014
D^0 decay multiplicity	0.004	0.003
Flavour tagging offsets	0.000	0.001
Flavour tagging mis-tag	0.000	0.009
Tracking resolution	0.015	0.010
Detector alignment	0.003	0.003
Fit method	0.012	0.010
Total	0.023	0.025

Table 2: Summary of systematic errors on the measured values of τ_{B^0} and Δm_d.

was obtained, where the errors are only statistical. The correlation between τ_{B^0} and Δm_d is -0.14. The fitted values of the other parameters were consistent with expectations from Monte Carlo simulations.

The distributions of reconstructed proper time t for opposite and same sign data events with $\Delta M < 0.17\,\text{GeV}$, together with the fit results, are shown in Figure 3. The fractions of mixed events R, corrected for the dilution due to mis-tagged events, are shown for the same ΔM regions in Figure 4, where the oscillation of signal $\bar{B}^0 \to D^{*+}\ell^-\bar{\nu}$ decays and the oscillation in the combinatorial background are clearly visible. The fit describes the data well, both in this mass region and in the high ΔM region dominated by combinatorial background. The discrepancy at high reconstructed proper times in the opposite sign sample (Figure 3(a)) is caused by imperfections in the resolution function (see Figure 2(f)) and is addressed as a systematic error.

6 Systematic Errors

Systematic errors arise from the uncertainties in the fit input parameters given in Table 1, the Monte Carlo modelling of the signal proper time resolution and backgrounds, the production flavour tagging performance and possible biases in the fitting method. The resulting systematic errors on the values of τ_{B^0} and Δm_d are summarised in Table 2 and described in more detail below.

Input quantities: The various numerical fit inputs were each varied according to the errors given in Table 1 and the fit repeated to assess the resulting uncertainties. The B_s oscillation frequency Δm_s was varied from the experimental lower limit of $9.1\,ps^{-1}$ [22] to $50\,ps^{-1}$, with no significant effect on the fit results.

$b \to D^{**}\ell\bar{\nu}$ decays: The systematic error due to the $b \to D^{**}\ell\bar{\nu}$ background is dominated by uncertainties in the rate of such decays, determined from the measured $Br(b \to D^{*+}\pi^-\ell\bar{\nu}X)$ as discussed in Section 5. To evaluate possible dependence in the $b \to D^{**}\ell\bar{\nu}$ decay model, the default JETSET model used in the simulation was reweighted according to the calculations of Leibovich et al. [25] as used in [8], with negligible change in the fit results. The relative contributions of B^+ and B^0 decays to this sample are expected to be predicted well by isospin symmetry, but the B_s contribution was scaled by 0.75 ± 0.25 relative to the isospin prediction to account for possible SU(3) flavour violation effects, as in [8]. Again, the resulting changes in the fit results were negligible.

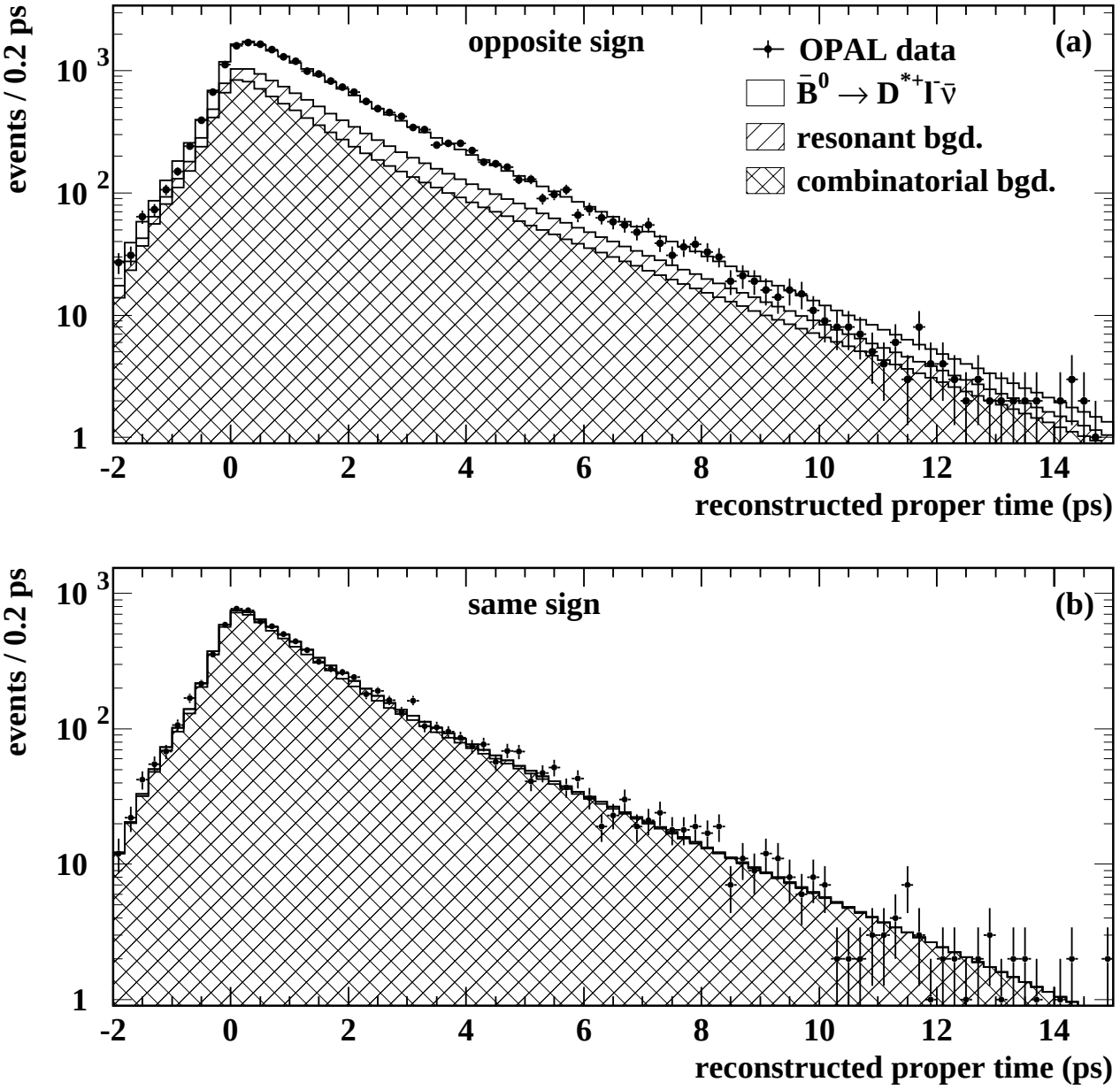

Figure 3: Distributions of reconstructed proper time t for (a) opposite sign and (b) same sign events with $\Delta M < 0.17\,\mathrm{GeV}$. The data are shown by the points with error bars and the expectation from the fit result by the histograms. The contributions from signal $\bar{\mathrm{B}}^0 \to \mathrm{D}^{*+}\ell^-\bar{\nu}$, resonant and combinatorial backgrounds are indicated.

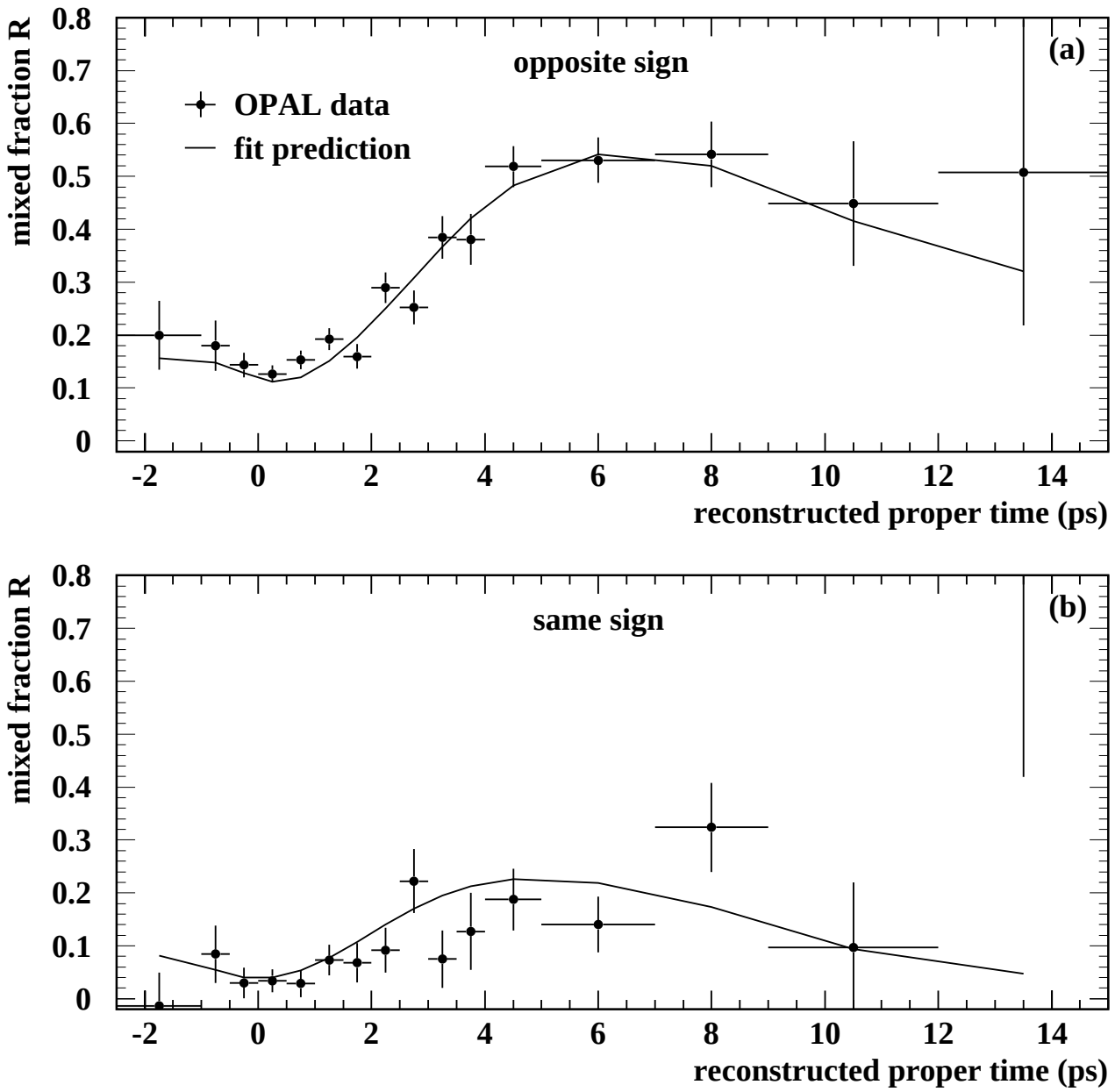

Figure 4: Corrected mixed event fractions R *vs.* reconstructed proper time t for (a) opposite sign and (b) same sign events with $\Delta M < 0.17\,\mathrm{GeV}$. The data are shown by the points with error bars and the expectation from the fit result by the solid line.

Other backgrounds: The backgrounds in fit source 3 from opposite sign $b \to D^{*+}\tau\bar{\nu}X$ and $b \to D^{*+}D_s^- X$, and same sign $D^{*+} \to D^0\pi^+$, $D^0 \to \ell^+ X$ decays have characteristic lifetimes of 1.87 ps and 1.42 ps respectively in the simulation. These values depend both on the true b hadron lifetimes and the mis-reconstruction of the apparent b hadron energy in these events, and were conservatively varied by ± 0.1 ps to assess systematic errors. These backgrounds also have oscillating components due to the contributions from B^0 decays (typically 60 % of the events). The systematic error was assessed by varying the B^0 fraction up to 100 % of the contribution from b hadrons, and repeating the fit.

b fragmentation: The effect of uncertainties in the average b hadron energy $\langle x_E \rangle = E_b/E_{beam}$ was assessed in Monte Carlo simulation by reweighting the events so as to vary $\langle x_E \rangle$ in the range 0.702 ± 0.008 as recommended by the LEP electroweak working group [26], and repeating the fit. This value is also consistent with a recent determination of $\langle x_E \rangle = 0.714 \pm 0.009$ from SLD [27]. The variation was implemented using the fragmentation functions of Peterson, Collins and Spiller, Kartvelishvili and the Lund group [28], and the largest observed variations were taken as systematic errors.

D^0 decay multiplicities: The b hadron energy reconstruction is sensitive to the B^0 decay multiplicity, which depends only on the D^0 decay for the B^0 decay channels of interest. The systematic error was assessed by varying separately the D^0 charged and π^0 decay multiplicities in the Monte Carlo simulation according to the measurements of Mark III [29]. The branching ratio $D^0 \to K^0$ or $\bar{K}^0$ was also varied according to its uncertainty [1]. The resulting uncertainties on τ_{B^0} and Δm_d from each variation were added in quadrature to determine the total systematic errors.

Production flavour tagging: The jet and vertex charge distributions Q_{opp}, Q_{same} and Q_{vtx} are not charge symmetric because of detector effects causing a difference in the rate and reconstruction of positive and negative tracks [30, 4]. These offsets were measured directly from the data as in [4], and their statistical uncertainties contribute to the systematic error on Δm_d.

The production flavour tagging mis-tag estimates must also be correct—*i.e.* that the values of Q correctly represent the mis-tag probabilities in the data. Excluding the events tagged by jet charge alone, the opposite flavour tags were checked in [4] to a precision of ± 2.6 %, using events tagged in both hemispheres. The same technique has been used to check the jet charge Q_{opp}, which was found to be correct to a precision of ± 10 %. The same hemisphere jet charge tag Q_{same} was also checked in [4] to ± 10 %. These uncertainties were translated into systematic errors on Δm_d by scaling the values of Q_T and Q_M and repeating the fit.

Tracking resolution: Uncertainties in the tracking detector resolution affect the time resolution for $\bar{B}^0 \to D^{*+}\ell^-\bar{\nu}$ and $\bar{B} \to D^{**}\ell^-\bar{\nu}$ events. The associated error was assessed in the simulation by applying a global 10 % degradation to the angular and impact parameter resolutions of all tracks, independently in the r-ϕ and r-z planes as in [13], and repeating the fit.

Detector alignment: The results are sensitive to the effective radial positions of the silicon detector wafers (both the positions of the detectors themselves and the positions of the charge collection regions within them), which are known to a precision $\pm 20\,\mu$m from studies of cosmic ray events [13]. The resulting uncertainty was assessed in Monte Carlo simulation by displacing one or both microvertex detector barrels by $20\,\mu$m and repeating the fit.

Fit method: The entire fitting procedure was tested on a fully simulated Monte Carlo sample six times bigger than the data, with true values of $\tau_{B^0} = 1.6$ ps and $\Delta m_d = 0.437\,\text{ps}^{-1}$. The fit gave the results $\tau_{B^0} = 1.604 \pm 0.012$ ps and $\Delta m_d = 0.440 \pm 0.010\,\text{ps}^{-1}$, in both cases consistent with the true values. The statistical errors on the fitted values were taken as systematic errors to account for possible biases in the fit. Additionally, the large Monte Carlo sample was reweighted

to change the values of τ_{B^0} and Δm_{d}, and the fit correctly recovered the modified values. To verify the correctness of the statistical errors returned by the fit, the large Monte Carlo sample was split into many subsamples, and the distribution of fitted results studied. The signal mass distribution $M_1(\Delta M)$ was varied to cover possible discrepancies in the Monte Carlo modelling of the signal mass spectrum (see Figure 1). The data fit was repeated changing the minimum reconstructed time cut to $-1.5\,\mathrm{ps}$ and the maximum to $10\,\mathrm{ps}$ (see Figure 3(a)), and varying the maximum mass difference ΔM between 0.20 and 0.25 GeV. Finally, the data was divided up into 5 subsamples according to the year of data taking. In all cases, consistent results were found, and no additional systematic error was assigned.

7 Conclusions

The lifetime and oscillation frequency of the B^0 meson have been measured using $\bar{\mathrm{B}}^0 \to \mathrm{D}^{*+}\ell^-\bar{\nu}$ decays selected with an inclusive technique. The results are:

$$\begin{aligned} \tau_{\mathrm{B}^0} &= 1.541 \pm 0.028 \pm 0.023\,\mathrm{ps}\,, \\ \Delta m_{\mathrm{d}} &= 0.497 \pm 0.024 \pm 0.025\,\mathrm{ps}^{-1} \end{aligned}$$

where in each case the first error is statistical and the second systematic. These results are consistent with other determinations of τ_{B^0} [4–6, 31, 32] and Δm_{d} [9, 17, 30, 33, 34], with the world averages of $\tau_{\mathrm{B}^0} = 1.54 \pm 0.03\,\mathrm{ps}$ and $\Delta m_{\mathrm{d}} = 0.470 \pm 0.019\,\mathrm{ps}^{-1}$ [22], and are in each case the most precise determinations to date.

The results presented here have been combined with the previous OPAL measurements of τ_{B^0} using neutral secondary vertices [4] and exclusively reconstructed $\mathrm{B}^0 \to \mathrm{D}^{(*)}\ell\bar{\nu}$ decays [31] and with measurements of Δm_{d} from single lepton [30], dilepton [17] and exclusively reconstructed D^{*+} decays [33], taking into account statistical and systematic correlations. The results

$$\begin{aligned} \tau_{\mathrm{B}^0} &= 1.538 \pm 0.025 \pm 0.023\,\mathrm{ps}\,, \\ \Delta m_{\mathrm{d}} &= 0.479 \pm 0.018 \pm 0.015\,\mathrm{ps}^{-1} \end{aligned}$$

were obtained, where again the first errors are statistical and the second systematic.

Acknowledgements

We particularly wish to thank the SL Division for the efficient operation of the LEP accelerator at all energies and for their continuing close cooperation with our experimental group. We thank our colleagues from CEA, DAPNIA/SPP, CE-Saclay for their efforts over the years on the time-of-flight and trigger systems which we continue to use. In addition to the support staff at our own institutions we are pleased to acknowledge the
Department of Energy, USA,
National Science Foundation, USA,
Particle Physics and Astronomy Research Council, UK,
Natural Sciences and Engineering Research Council, Canada,
Israel Science Foundation, administered by the Israel Academy of Science and Humanities,
Minerva Gesellschaft,
Benoziyo Center for High Energy Physics,
Japanese Ministry of Education, Science and Culture (the Monbusho) and a grant under the Monbusho International Science Research Program,
Japanese Society for the Promotion of Science (JSPS),
German Israeli Bi-national Science Foundation (GIF),

Bundesministerium für Bildung und Forschung, Germany,
National Research Council of Canada,
Research Corporation, USA,
Hungarian Foundation for Scientific Research, OTKA T-029328, T023793 and OTKA F-023259.

References

[1] Particle Data Group, C. Caso et al., Eur. Phys. J. C3 (1998) 1.

[2] See for example: I.I. Bigi and P.J. Dornan, Phys. Rep. 289 (1997) 1 and references therein.

[3] See for example: K. Österberg, 'Measurement of $|V_{\rm cb}|$ and $|V_{\rm ub}|$ at LEP', to appear in proceedings of the International Europhysics Conference on High Energy Physics, Tampere, Finland, 15-21 July 1999, published by IOP (Bristol, UK).

[4] OPAL collaboration, G. Abbiendi et al., Eur. Phys. J. C12 (2000) 609.

[5] DELPHI collaboration, W. Adam et al., Z. Phys. C68 (1995) 363;
L3 collaboration, M. Acciarri et al., Phys. Lett. B438 (1998) 417;
SLD collaboration, K. Abe et al., Phys. Rev. Lett. 79 (1997) 590.

[6] DELPHI collaboration, P. Abreu et al., Z. Phys. C74 (1997) 19.

[7] DELPHI collaboration, P. Abreu et al., Z. Phys. C71 (1996) 539.

[8] OPAL collaboration, G. Abbiendi et al., 'Measurement of $|V_{\rm cb}|$ using $\bar{\rm B}^0 \to {\rm D}^{*+}\ell^-\bar{\nu}$ decays', CERN-EP-2000-032, accepted by Phys. Lett. B.

[9] DELPHI collaboration, P. Abreu et al., Z. Phys. C76 (1997) 579.

[10] See for example: M. Neubert, Int. J. Mod. Phys. A. 11 (1996) 4173.

[11] OPAL collaboration, K. Ahmet et al., Nucl. Instrum. Methods A305 (1991) 275;
P.P. Allport et al., Nucl. Instrum. Methods A324 (1993) 34;
P.P. Allport et al., Nucl. Instrum. Methods A346 (1994) 476;
S. Anderson et al., Nucl. Instrum. Methods 403 (1998) 326.

[12] T. Sjöstrand, Comp. Phys. Comm. 82 (1994) 74.

[13] OPAL collaboration, G. Abbiendi et al., Eur. Phys. J. C8 (1999) 217.

[14] OPAL collaboration, R. Akers et al., Z. Phys. C63 (1994) 197.

[15] OPAL collaboration, P.D. Acton et al., Z. Phys. C58 (1993) 523.

[16] OPAL collaboration, P.D. Acton et al., Z. Phys. C59 (1993) 183;
OPAL collaboration, R. Akers et al., Phys. Lett. B338 (1994) 497.

[17] OPAL collaboration, R. Akers et al., Z. Phys. C66 (1995) 555.

[18] OPAL collaboration, K. Ackerstaff et al., Eur. Phys. J. C2 (1998) 213;
OPAL collaboration, G. Abbiendi et al., Eur. Phys. J. C12 (1999) 567.

[19] OPAL collaboration, K. Ackerstaff et al., Z. Phys. C73 (1997) 397.

[20] OPAL collaboration, K. Ackerstaff et al., Eur. Phys. J. C5 (1998) 379.

[21] OPAL collaboration, R. Akers et al., Phys. Lett. B327 (1994) 411.

[22] Particle Data Group, 1999 off-year partial update for the 2000 edition available on the PDG WWW pages at `http://pdg.lbl.gov/`.

[23] ALEPH collaboration, D. Buskulic et al., Z. Phys. C73 (1997) 601.

[24] OPAL collaboration, K. Ackerstaff et al., Eur. Phys. J. C1 (1998) 439.

[25] A. Leibovich, Z. Ligeti, I. Stewart and M. Wise, Phys. Rev. D57 (1998) 308.

[26] The LEP collaborations, ALEPH, DELPHI, L3 and OPAL, Nucl. Instrum. Methods A378 (1996) 101.
Updated averages are described in 'Presentation of LEP Electroweak Heavy Flavour Results for Summer 1998 Conferences', LEPHF 98-01 (see `http://www.cern.ch/LEPEWWG/heavy/`).

[27] SLD collaboration, K. Abe et al., Phys. Rev. Lett. 84 (2000) 4300.

[28] C. Peterson, D. Schlatter, I. Schmitt and P. Zerwas, Phys. Rev. D27 (1983) 105;
P. Collins and T. Spiller, J. Phys. G11 (1985) 1289;
V.G. Kartvelishvili, A.K. Likhoded and V.A. Petrov, Phys. Lett. B78 (1978) 615;
B. Anderson, G. Gustafson and B. Söderberg, Z. Phys. C20 (1983) 317.

[29] MARK III collaboration, D. Coffman et al., Phys. Lett. B263 (1991) 135.

[30] OPAL collaboration, K. Ackerstaff et al., Z. Phys. C76 (1997) 401.

[31] OPAL collaboration, R. Akers et al., Z. Phys. C67 (1995) 379.

[32] ALEPH collaboration, D. Buskulic et al., Z. Phys. C71 (1996) 31;
CDF collaboration, F. Abe et al., Phys. Rev. D58 (1998) 092002;
CDF collaboration, F. Abe et al., Phys. Rev. D57 (1998) 5382;
DELPHI collaboration, P. Abreu et al., Z. Phys. C68 (1995) 13.

[33] OPAL collaboration, G. Alexander et al., Z. Phys. C72 (1996) 377.

[34] ALEPH collaboration, D. Buskulic et al., Z. Phys. C75 (1997) 397;
CDF collaboration, F. Abe et al., Phys. Rev. Lett. 80 (1998) 2057;
CDF collaboration, F. Abe et al., Phys. Rev. D59 (1999) 032001;
CDF collaboration, F. Abe et al., Phys. Rev. D60 (1999) 072003;
CDF collaboration, F. Abe et al., Phys. Rev. D60 (1999) 051101;
CDF collaboration, F. Abe et al., Phys. Rev. D60 (1999) 112004;
L3 collaboration, M.Acciarri et al., Eur. Phys. J. C5 (1998) 195.